JOURNAL OF MATERIALS SCIENCE **34** (1999) 5733–5742

A technique for the fabrication of fully dense Ca-rich plagioclase (An_{70}-An_{100}) samples suitable for studying the plastic rheology of bytownite (An_{80})

A. S. WENDT*
Laboratoire de Tectonophysique, Université Montpellier 2 Place Eugène Bataillon, 34095 Montpellier France
E-mail: a.wendt@ucl.ac.uk

D. L. OLGAARD‡
Geologisches Institut, ETH-Zentrum Sonneggstrasse. 5, 8092 Zurich, Switzerland
E-mail: David.L.Olgaard@exxon.sprint.com

D. MAINPRICE
Laboratoire de Tectonophysique, Université Montpellier 2 Place Eugène Bataillon, 34095 Montpellier France
E-mail: david@dstu.univ-montp2.fr

Two different types of solid samples of bytownite ($Ca_{0.7}Na_{0.3}Al_2Si_2O_8$ to $Ca_{0.9}Na_{0.1}Al_2Si_2O_8$) composition were fabricated from synthetic crystal and glass powders. The crystal and the glass powders were produced by crystallisation or melting of a gel of bytownite composition. Cold pressing under vacuum followed by hot isostatic pressing (hip) of the powders produced fully dense samples composed either of 100% bytownite crystals or of 90% bytownite crystals and 10% bytownite glass. The cold-pressed samples were composed of a matrix of nanometer sized bytownite needles and larger crystals of up to 3 μm in size. During hot pressing the grain sizes in the matrix increased slightly while larger crystals increased to close to 4 μm. The rheological behaviour of the hot isostaticly pressed samples for cases of tri axial compression and torsion was tested in a gas confining deformation apparatus at high temperature and confining pressure. Grain growth was observed during the deformation experiments. The maximum flow stress was typically less than 200 MPa and was attained by sample strain of 10% during axial compression and a shear strain of 1.0 during torsion. The resulting microstructures were dominated by fibrous grains for the compressive deformation and by more round-shaped grain boundaries during torsion. Both type of experiments induced a preferred shape and crystallographic orientation. © *1999 Kluwer Academic Publishers*

1. Introduction

Plagioclase ($CaAl_2Si_2O_8$ to $NaAl_2Si_2O_8$) is one of the major constituents of the Earth's crust, and therefore the knowledge of its mechanical properties is of considerable interest to earth scientists seeking to understand the deformation behaviour of the upper lithosphere. At mid to lower crustal depths (approximately 30 to 70 km), plagioclase deforms, at least in part, by plastic deformation processes [e.g. 1, 2]. However, at present the knowledge of the plastic deformation behaviour of plagioclase is very limited.

Previous experimental studies of the mechanical properties of plagioclase concentrated primarily on the deformation of fine-grained rocks of the calcium end member of plagioclase (anorthite).

Seifert (1969) [3] and Borg and Heard (1969, 1970) [4, 5] observed that natural plagioclase did not deform plastically when investigated experimentally at high temperature (700 °C) and medium confining pressures (500 MPa). Cracks and microcracks occurred at temperatures up to 1000 °C [6]. Brittle flow of anorthite rocks has been observed by Tullis and Yund (1992) [7] at modest temperatures (300 °C to 600 °C) and high pressure (about 750 MPa) and at low temperature (250° to 300 °C) and very high pressures (1000 to 1500 MPa). Increasing temperature (>300 °C) [8, 9] at

* *Present address:* Rock & Ice Physics Laboratory, Department of Geological Sciences, University College London, Gower Street, London WC1E 6BT, UK.

‡ *Present address:* Exxon Production Research Company, Room N-343, P.O. Box 2189, Houston, TX 77252-2189 USA.

pressures <1500 MPa produced a transition from brittle flow to recrystallisation-accommodated dislocation creep. Mechanical twinning occurred at a temperature of about 600 °C. Dislocation activities have been observed at temperatures higher than 700 °C, and the onset of recrystallisation was reported at 800 °C [7] while the movements of the dislocations can be enhanced by trace amounts of water [10, 11]. Steady state dislocation creep was observed in experiments at confining pressures higher than 750 MPa for temperatures higher than 700 °C. The transition from dislocation creep to diffusion creep may be related to dynamic recrystallisation [12–14], grain size sensitive flow or other strain softening mechanisms promoting strain localisation [15, 16].

Given the complicated rheological behaviour of natural and synthetic anorthite, an investigation of the rheological properties of calcic plagioclase rocks is essential, under circumstances were the parameters which influence the mechanical behaviour of the samples, e.g. composition and microstructures, are carefully controlled. In this study, we fabricate bytownite ($Ca_{0.7}Na_{0.3}Al_2Si_2O_8$ to $Ca_{0.9}Na_{0.1}Al_2Si_2O_8$ corresponds to "Anorthite$_{70}$ (An_{70}) to Anorthite$_{90}$ (An_{90})") samples of controlled microstructures in order to develop specimen which allow to test the plastic rheology of Ca-rich plagioclase.

2. Sample Preparation

Crystalline bytownite and bytownite crystals plus glass of bytownite composition samples were fabricated in order to control chemical purity, chemical homogeneity, grain size and glass-fraction of the specimens. Both crystals and glass were prepared by a solution-gelation (sol-gel) procedure using the appropriate quantities of all the chemicals element required by the crystals structural formula $Ca_{0.8}Na_{0.2}Al_2Si_2O_8$. A true one-phase solution of tetraethylorthosilicate (T.E.O.S.), water and ethanol, two carbonates ($CaCO_3$, Na_2CO_3) and aluminium was prepared and transformed (sol-gel) to a rigid 2-phase system of solid silica and solvent-filled pores. The chemicals were obtained from the companies Johnson Matthey (France) and Riedel de Haën (France). The calcium carbonate, the sodium carbonate and the aluminium were powders of Specpure quality and T.E.O.S. was used as the liquid tetraethoxysilane 99%. We also used high purity nitric acid, absolute ethanol and ultrapure ammonium hydroxide. The total impurity content (e.g. all cations other than Ca, Na and Al and Si) of the final gel powder corresponded to the impurities of the initial raw material and was less than 0.001 wt %. After precipitation, the gel was dried and heated to produce either a crystalline powder or a powder of an amorphous phase with bytownite-composition.

2.1. Sol-Gel preparation

Dried Na_2CO_3 (0.42845 g) and $CaCO_3$ (3.2367 g) powders were weighed to the absolute quantities required by the structural formula of bytownite based on a Si supply corresponding to 20 ml T.E.O.S. Overnight drying of the powders was performed at 100 °C for exact weighing. Both powders were transferred to a 500 ml teflon beaker and then converted to nitrates by adding heated (80 °C) nitric acid until a perfectly clear solution was obtained. To avoid any loss of the powders during weighing and transferring them to the teflon beaker weighing was achieved under static-free air conditions. The corresponding quantity of aluminium (36.6 ml) was then added to the warmed solution as aluminium nitrate dissolved in ultrapure water (aluminium titrate) (>99.99%). SiO_2 was added as the liquid T.E.O.S. (20 ml) washed into the beaker simultaneously with sufficient (10 to 20 ml) ultra pure ethanol (>99.99%). Enough ethanol (20 ml) has to be provided to render the T.E.O.S. and the nitrate solution miscible (approximately one part of alcohol to one part of T.E.O.S. per nitrate solution). The resulting solution was homogeneous and contained all the elements of bytownite in the required proportions. Ammonium hydroxide (35 ml) was added to precipitate the silica. During the whole process of mixing, and for at least 15 min afterwards, the solution was continuously warmed at 50 °C and stirred. By the end of the 15 min gelling was complete. The result was a stiff gel with no supernatant solutions.

To ensure complete precipitation before drying, the gel was left overnight at room temperature. Drying was performed on a hot plate starting at a temperature of 100 °C which was ramped in steps of 50 °C up to 200 °C for 2 h. The pre-dried gel was then transferred to a platinum crucible for firing it in an oven at 550 °C for 2 h to decompose the nitrates. Once dried, the gel was ready for grinding, crystallisation or melting to a glass.

2.2. Crystallisation and melting

The ground gel was transferred into a flat open platinum crucible to a high temperature furnace. Different crystallisation temperatures below the melting temperature (1490 °C) of bytownite were tried to prevent fractional crystallisation. The crystallisation was performed in a high temperature furnace (Keramon 30691) at temperatures of 840 °C to 970 °C for 3 days. The heating of the furnace to the required temperature was at a rate of 30 °C/min. A temperature of 940 °C produced the best crystallisation results. This condition was found to crystallise a >98% dense and chemically homogeneous material compared to crystallisation at lower or higher temperatures which produced more porous and chemically inhomogeneous material for the same time span of crystallisation. The material was cooled to 500 °C after crystallisation at a rate of 30 °C/min and was then quenched in water.

Melting of the dried gel was performed in a horizontal high temperature furnace (Pyrox 1800) at a constant temperature of 1570 °C for 4 days. The heating to 1570 °C was again at a rate of 30 °C/min and crystallisation during cooling was prevented by quenching the melt in water.

Microprobe analyses showed that both synthetic powders, the crystalline and the amorphous, were of homogeneous chemical composition corresponding

TABLE I Microprobe analyses of the initial powder material (glass phase, crystals) and of the hot pressed and deformed material. Structural formulae were calculated based on 32 O

	Glass Phase: Conc. %			Crystalline Phase: Conc. %					
Initial Material									
Microprobe analysis data									
Na_2O	2.138	1.962	2.239	1.352	1.868	1.523	2.05	1.984	1.651
MgO	0	0	0	0	0	0	0	0	0
Al_2O_3	33.51	33.6	33.66	33.77	33.56	38.38	32.73	34.06	31.98
SiO_2	48.43	47.79	47.8	45.64	47.94	42.74	47.77	48.72	46.51
FeO	0	0	0	0.04	0	0.23	0	0	0
K_2O	0.169	0	0.509	0.023	0	0.009	0	0	0
CaO	15.03	13.5	16.27	18.41	16.54	16.67	17.4	16.15	16.84
Total	99.339	96.84	100.48	99.246	99.91	99.346	99.9	100.9	96.974
Structural formulae for samples 1 to 9									
Ca	0.74	0.7	0.8	0.9	0.8	0.8	0.86	0.8	0.8
Na	0.19	0.2	0.22	0.15	0.17	0.15	0.19	0.15	0.15
Al	1.81	1.85	1.8	1.9	1.8	1.9	1.78	1.8	1.8
Si	2.23	2.23	2.19	2.1	2.2	1.83	2.23	2.34	2.34
O	8	8	8	8	8	8	8	8	8
Sintered and Deformed Material									
Microprobe analysis data									
Na_2O	2.324	3.293	3.007	2.681	4.14	2.208	2.41	2.292	2.684
MgO	0	0	0	0	0	0.037	0	0	0
Al_2O_3	34.36	30.42	31.49	32.52	28.51	32.04	33.31	33.75	33.39
SiO_2	47.55	50.69	49.06	47.89	53.06	47.92	48.24	47.73	47.68
FeO	0.013	0.097	0.014	0	0.021	0.016	0.01	0.007	0
K_2O	0	0.004	0	0.016	0.019	0	0.008	0	0.012
CaO	14.69	14.12	15.13	15.52	14.09	17.07	15.55	15.25	15.15
Total	98.935	98.619	98.701	98.629	99.847	99.293	99.528	99.035	98.914
Structural formulae for samples 1 to 9									
Ca	0.73	0.7	0.83	0.8	0.7	0.85	0.77	0.75	0.75
Na	0.21	0.3	0.27	0.24	0.38	0.22	0.22	0.22	0.22
Al	1.87	1.7	1.7	1.8	1.54	1.71	1.8	1.83	1.66
Si	2.19	2.3	2.25	2.2	2.4	2.2	2.2	2.2	2.2
O	8	8	8	8	8	8	8	8	8

The three columns for the glass phase and the six columns for the crystalline phase represent samples 1 to 9.

to a bytownite (An_{80}) (Table I). Scanning electron microscope (SEM) images showed the crystalline structure of the crystallized powder (Fig. 1a,b). The particles in the crystallized powders comprised crystals of about 3 μm in a matrix of crystals less than 400 nm in size. The larger crystals were frequently twinned (distance between twin planes about 100 nm) (Fig. 1b). The melting produced a pore- and inclusion free glass (Fig. 1c). The water content of both powders was determined by infrared spectrometry analyses and revealed an average amount of 89 ppm H/Si for the crystal powder and 41 ppm H/Si for the glass powder (Table II).

TABLE II Data of infrared spectroscopy (FTIR). Calculations see text

Spectrometer	Bomen DA3
Source	Globar
Separator	KBr (bromide of Potassium)
Detector	MCT (Mercury, Cadmium, Telluric)
Measuring	By analytical microscope Spectratech
Resolution	4 cm^{-1}
Beam size	3.5 mm
Studied zone	80 μm × 80 μm
No. of scans	200
Concentrations of OH in test samples	
Initial material:	
Crystal powder	89 ppm H/Si
Glass powder	41 ppm H/Si
Hot pressed and/or deformed material:	
Hot pressed	0.02 ppm H/Si
Test 2	0.04 ppm H/Si
Test 5	0.08 ppm H/Si
Test 6	0.02 ppm H/Si
Test 7	0.03 ppm H/Si

2.3. Cold pressing

First, the powders were dried at 200 °C for 24 h prior to pressing. They were then packed into a tubular iron jacket (1 mm thick walls, 10 mm in diameter) to a height of 25 mm. The jackets were capped at each end with 1mm thick iron discs. Cold pressing of the crystalline and amorphous powder was performed in a vacuum chamber which was designed to accept a hydraulic piston loading apparatus. The piston slides into the vacuum chamber through a tight O-ring seal and presses two freely moving iron-pistons in a split-die to compress the sample powder. Loading was performed under vacuum conditions to keep the pore space and the particle surfaces of the samples free from atmospheric water. An axial load of 753 MPa (maximum load before rupture) was applied to the specimen of loose powder for 15 min. Vacuum pressure conditions corresponded

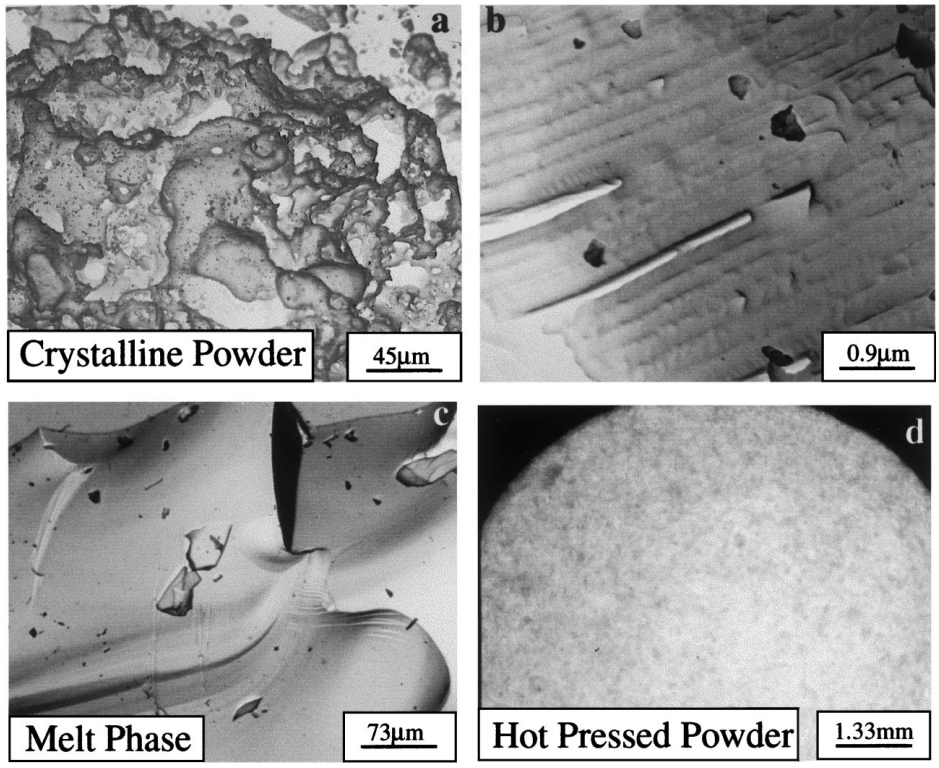

Figure 1 SEM images of the crystallised powder (a), of a large crystal with narrow twin planes (b), of the bytownite melt phase (c); (d) lens photograph of the hot pressed powder.

10^{-2} bar. During the cold pressing the density of the sample increased to 80%.

2.4. Hot isostatic pressing (HIP)

All of the polycrystalline cold pressed samples were individually isostaticly hot pressed at 1200 °C and 300 MPa from 3 to 5 h in the triaxial gas confining deformation apparatus (Paterson apparatus, [17]), later used to deform them. Temperature and pressure were increased at rates of approximately 30 °C/min and 8 MPa/min, respectively. Before hot pressing, the short iron jackets containing the cold-pressed powder samples were carefully machined to ensure parallelism of their ends. Then they were sealed into long jackets of iron together with solid aluminium-oxide spacers and a solid aluminium-oxide piston at each end. Sample and spacers then have a total length of 26 mm, the whole assemblage of iron jacket, forcing pistons, spacers and sample being 205 mm long. The long iron jackets were carefully squeezed around spacers and powder sample to ensure a tight fit. The progressive changes in the sample length were measured during the hot-pressing by monitoring the contact positions ('hit-point') of the loading piston of the Paterson rig and the sample through time to establish the densification rate until the final density. Fig. 2 shows that densification proceeded rapidly at first until 93%, then

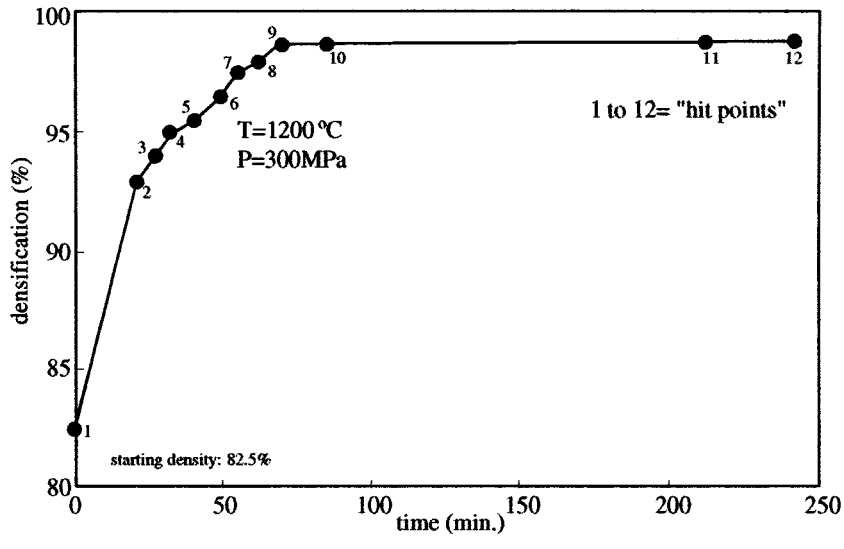

Figure 2 A typical densification versus time curve for hot isostatic pressing.

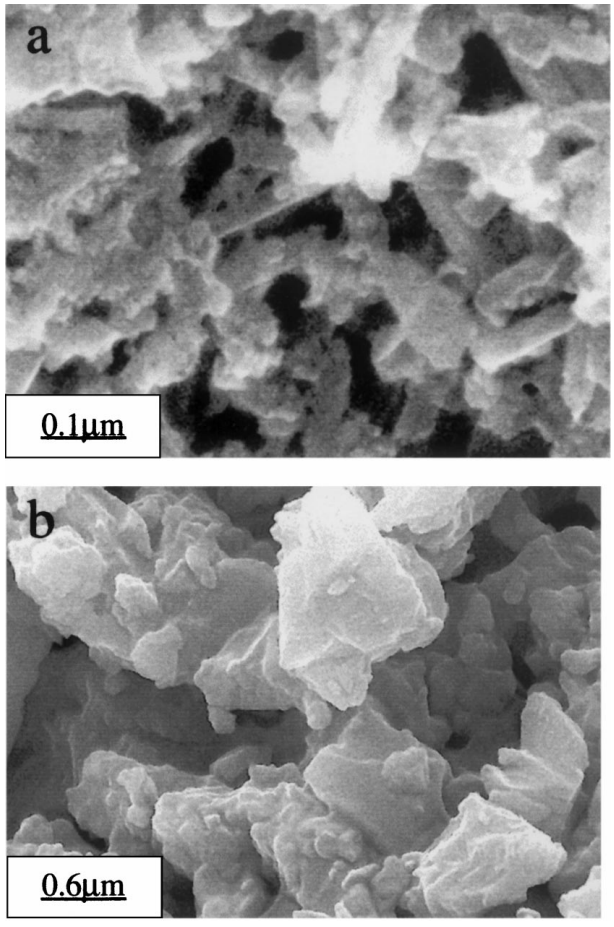

Figure 3 SEM images of the ultra-fine matrix composed by needles (a) and/or plates (b) taken in the hot pressed sample.

slowed until it had virtually stopped. In practice, hot pressing was terminated when there was no measurable change in length over the space of one hour. After hot pressing one sample was removed from the machine to examine the microstructures induced during sintering (test 1). Fig. 1d shows the surface perpendicular to the long axis of the sample after hot pressing. In all other cases, the deformation experiment was performed immediately after hot pressing. We obtained 4 good samples for the deformation test with lengths from 11.9 mm to 16.5 mm and a diameter of 8.8 mm.

Hot pressing enhanced the bimodality of the grain size distribution with a matrix composed of needle-shaped or plate-like crystals with lengths less than 600 nm (Fig. 3) containing larger crystals of up to 5 μm in size. Larger portions of bytownite exhibit after hot pressing, undulose extinction, serrated grain boundaries and subgrains (Fig. 4). Where individual bytownite needles or plates in the matrix were large enough to be separately distinguished, they revealed regular long sides with rounded edges.

3. Analytical techniques

The characterisation of the microstructures of the samples was carried out using secondary electron imaging on a Scanning Electron Microscope (SEM, Cambridge Instruments, Stereoscan 360, JEOL JSM-6300F) and

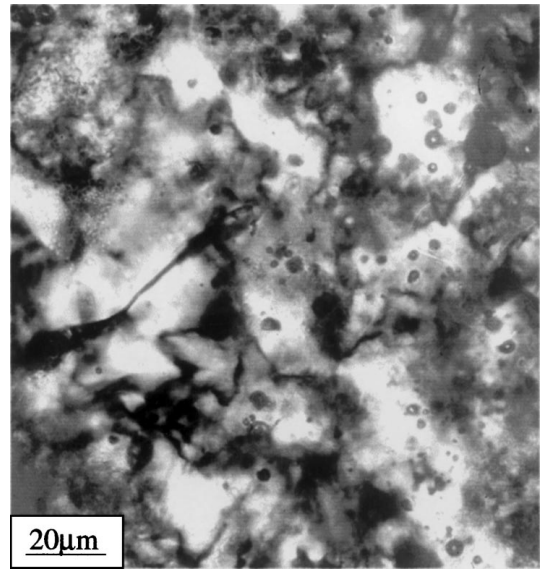

Figure 4 Micrograph taken under crossed polarisators of larger grain portions of bytownite after hot pressing. Grain boundaries seem large because of the superposition of several grains. The small dark dots are oxide impurities coming from the iron jacket.

optical microscopy. At the end of a hot-pressing or deformation run, the samples were prepared for SEM analyses by using cut and platinum coated sample surfaces perpendicular and parallel to the long axis of the specimens. Thin sections were prepared from the specimen deformed in torsion. The thin sections were oriented at 120° to each other and parallel to the long axis of the twisted specimen. They allowed to investigate the maximum grain elongation (function of the angular displacement of the sample). The grain size was measured using the linear intercept method on SEM micrographs. The chemical composition of the specimen was determined by electron microprobe (Camebax). Crystal defects and submicroscopical structures were observed and identified with a transmission electron microscope (TEM) (JEOL 200 CX at 120 kV) using double-polished thin sections taken perpendicular to the principal stress axis. TEM foils were prepared by ion milling the thin sections prepared from the bulk samples. Fourier Transform Infrared (FTIR) Spectroscopy (Bomen DA3) was used to determine the water content in the sintered and the deformed samples. Transmission FTIR measurements were made on thin sections of the specimens. Specific spectra were taken at wave numbers in the range 3000–3700 cm^{-1}. The infrared method for hydroxyl determination has been based on the formulae

$$c = K/\varepsilon \tag{1}$$

and

$$\varepsilon = 1/I \int K(v)\, d = \Delta/I \tag{2}$$

where c is the molar concentration, K is the absorption coefficient (equals the maximum ($K_{\max}$) of the absorption band when (1) is used), v is the wave number (reciprocal of wavelength), Δ is the integral absorption

coefficient, and ε and I are constants called the molar absorption and the integral molar absorption coefficient, respectively. The physical basis underlying these formulae and a discussion of the nomenclature is given at length by Paterson (1982) [18].

4. Mechanical tests on the hip-ed bytownite samples

We report here deformation experiments performed on the synthetic material in order to test if the material is suitabel for studying the plastic deformation behaviour of Ca-rich plagioclase.

Four deformation experiments were performed on the cylindrical bytownite samples to investigate their rheological behaviour. The mechanical tests were carried out at axial compression and torsion at high confining pressure (300 MPa) and high temperature (1150 °C, 1200 °C). Strain rates were 10^{-5} s^{-1}. The experiments were performed in the gas confining Paterson deformation apparatus of the Geologisches Institut of ETH Zurich (see detailed description in [17, 19–22]). For all experiments temperatures were calibrated to a gradient of 3 °C over a length of 50 mm around the specimen. The torsion experiment was performed using a torsion actuator which has been installed on the gas confining Paterson apparatus. The torsion actuator of the Paterson system applies a torque to the top end of the specimen assembly in order to twist it anticlockwise while its angular position was fixed at the bottom end. A detailed description of the torsion system and first results on torque deformation can be found elsewhere [23–27]. The specimen assembly used during torsion was similar to the assembly used for hot pressing and axial compression. The strain rate during torsion was measured as the rate of angular displacement at the surface of the specimen

$$d\theta/d\mathrm{t} = d\gamma/d\mathrm{t} \cdot 1/R \qquad (3)$$

with (θ-angular displacement, γ-shear, 1-specimen length, R-specimen radius).

The maximum strain-rate for torsion was measured at the outer surface of the sample and was equal to 10^{-5} s^{-1}. The specimen dimensions were 9 mm in diameter and 5.5 mm in length. Microstructural examinations was carried out on 2 surfaces cut parallal to the cylinder axis. On these surfaces the deformation varied due to the different radial depth of the surface and the different orientation of the shear direction with respect to the surface plane normal.

4.1. Experiments

All together four successful mechanical tests were performed. The deformation conditions and the strain attained for the samples are reported in Table III. The data of the hot isostatic pressing and the deformation data were corrected for the change in sample cross section area with increasing strain assuming constant volume deformation (here equal to shortening), and for the known apparatus distortion under load and for the load supported by the iron jackets. The oxygen fugacity of the samples was not buffered externally, and was probably set by the iron jacket at Fe-FeO.

The stress-strain curves of the three compression experiments (test 2, test 5, test 6) and of the torsion experiment (test 7) are shown in Fig. 5a. All three compression experiments developed a maximum flow stress before in two cases (test 5, test 6) the samples began to work soften. The maximum flow stress reached was 135 MPa for 7.5% of strain during test 2, 115 MPa for 10% of strain during test 5 (conducted on a sample composed of crystals and glass) and 185 MPa for 9.5% of strain during test 6. The flow stress versus strain curves for axial compression showed that the sample deformed at 1150 °C (test 5) was stronger than the samples deformed at 1200 °C (test 2, test 6). The melt-bearing sample was weaker at 1200 °C than the melt-free sample.

The stress-strain curves of the torsion test is shown in Fig. 5b. Deformation in the torsion regime revealed maximum flow at a flow stress of 160 MPa for an experimentally measured shear strain of about 1.0 ($\varepsilon = 58\%$) (Fig. 5b). The flow stress versus shear strain evolution during torsion showed that the sample strain hardened significantly at first followed by weakening which was followed by a weak approximately linear hardening.

4.2. Water content

The water content of the hot pressed and deformed samples was measured by Infrared Spectroscopy (Fig. 6). The water content is close to the limit of detectability and lies between 0.02 ppmH/Si to 0.08 ppmH/Si (Table II). The absolute water concentration of any sample was calculated by determining the molar absorption coefficient ($K(\mathrm{cm}^{-1})$) integrated over the region

TABLE III Experimental conditions and results for the experiments of this study (S = Sintering, aC = axial Compression, T = Torsion)

Sample	T(°C)	P(MPa)	Strain rate (s^{-1})	Composition	Strain	max. Stress (MPa)
Test 1: S	1200	300	1×10^{-5}	Crystals	/	/
Test 2: S & aC	1200	300	1×10^{-5}	Crystals	7.5%	135
Test 3:			Failed			
Test 4:			Failed			
Test 5: S & aC	1200	300	1×10^{-5}	Crystals & Melt	10%	115
Test 6: S & aC	1150	300	1×10^{-5}	Crystals	9.5%	185
Test 7: T	1200	300	1×10^{-5}	Crystals	$\gamma = 1$ ($\varepsilon = 58\%$)	160

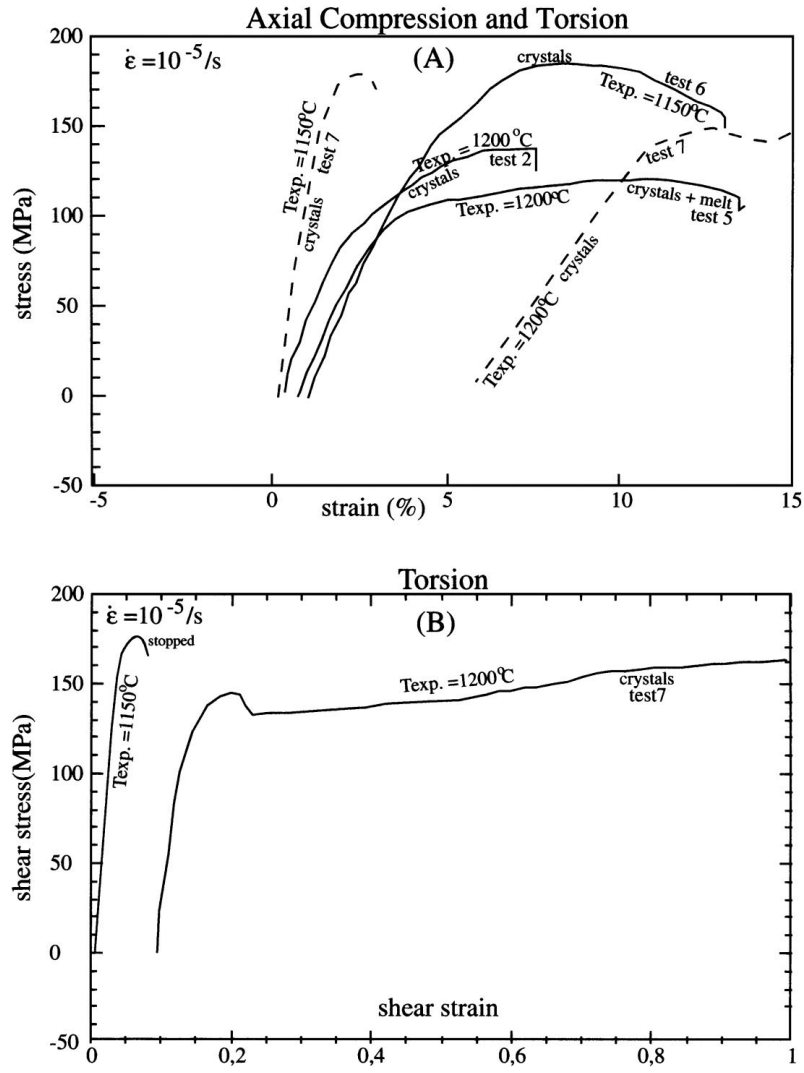

Figure 5 (A) Stress difference versus strain curves for the high temperature axial compression and torsion tests on the one-phase and two-phase bytownite samples. The strain rate was calculated from the axial displacement of the loading piston. (B) Shear stress versus shear strain curve for the high temperature torsion experiment. The strain rate was calculated from the rate of angular displacement. The confining pressure for all the 4 tests was equal to 300 MPa.

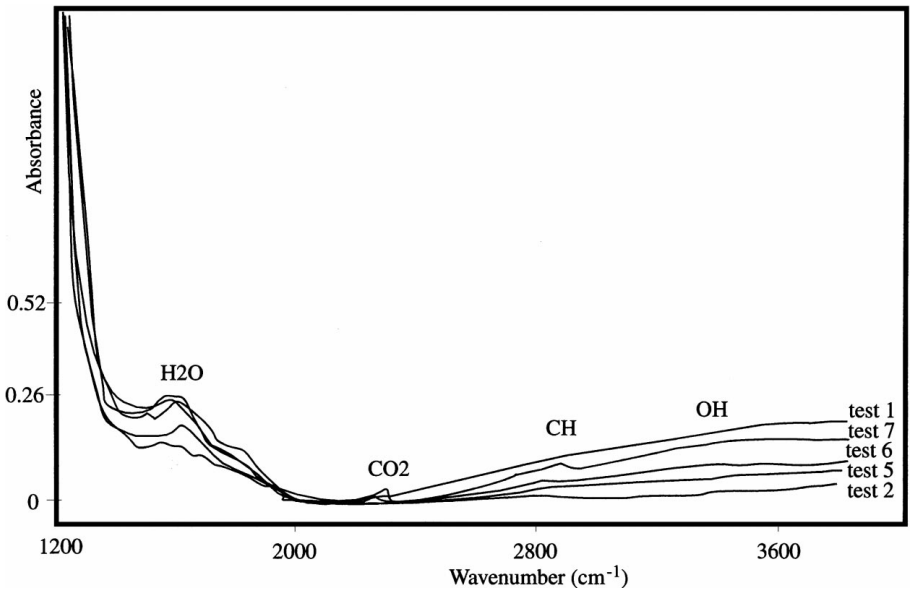

Figure 6 Absorbance of water in the deformed samples. Values obtained by FTIR measurements on thin sections.

between the wave numbers 3000 cm^{-1} and 3700 cm^{-1} obtained from the infrared measurements:

$$C_{OH} = 1/\varepsilon^* \int_{3000}^{3700} K(v)\,dv = \Delta/\varepsilon^* \qquad (4)$$

with $\varepsilon^*_{OH} = 210001*$ $mole^{-1}*$ cm^{-2} [19].

Generally, the water content was so low that we considered the specimen as being almost dry.

5. Microstructures induced by deformation

5.1. Axial compression

Axial compression induced a very heterogeneous strain distribution and produced fibrous crystals and strong grain growth. Large single crystals and crystal aggregates increased their size up to 5 μm. Domains composed of recrystallised grains with grain sizes of about 600 nm appeared at about 45° to the applied principal stress ($\sigma 1$). An unrecrystallised matrix was still present and composed of needle-shaped crystallites and plate-like crystallites with sizes up to 800 nm. Neither the needles (Fig. 7d) nor the plates showed any sign of intracrystalline plasticity, but in most areas individual particles are difficult to resolve because they were smaller than 600 nm.

Microstructural differences were distinguished between the tests of different compositions. The fully crystalline samples showed after deformation fibre aggregates including radially divergent fibres, bundles, rosettes, and spherulites composed of randomly divergent fibres and crystallographically controlled interpenetrating fibres (Fig. 7a,b). The fibre aggregates were slightly flattened perpendicular to the applied principal stress ($\sigma 1$) or oriented in diffuse conjugate shear bands at 45° to the applied principal stress ($\sigma 1$). The growth of individual fibres parallel to the *c*-axis of bytownite within the aggregations varied and gave the fibre bundles different optical textures. In any one growth direction the closely spaced fibres in each bundle remained approximately parallel to one another. Large crystals and recrystallised grains are irregular in shape, often undulose and twinned on a fine-scale (Fig. 7c). Dislocations were rarely observed and it is suggested that the lack of important dislocation creep processes during twinning resulted from grain growth under load. The twinned grains appeared locally and alternated irregularly with the fibrous domains throughout the specimen.

The glass bearing bytownite sample (test 5) exhibited similar microstructures as the samples without melt. The glass phase formed pockets and seemed trapped also along grain boundaries. The glass in the pockets crystallised to a multitude of small crystals of about 1 μm in size constituting the crystallisation nucleus for exaggerated fibres growth to aggregates which can reach more than 500 μm in size with fibres projecting radially outward from the small crystals (Fig. 7b). Those aggregates are oriented in diffuse conjugated shear bands at 45° to the applied principal stress ($\sigma 1$). Melt on grain boundaries probably crystallised into fibres and the same type of ultrafine matrix, and it was no longer possible to distinguish it from the pre-existing material.

5.2. Torsion

The torsion experiment allowed the study of microstructures at large (shear) strains. The iron jacket

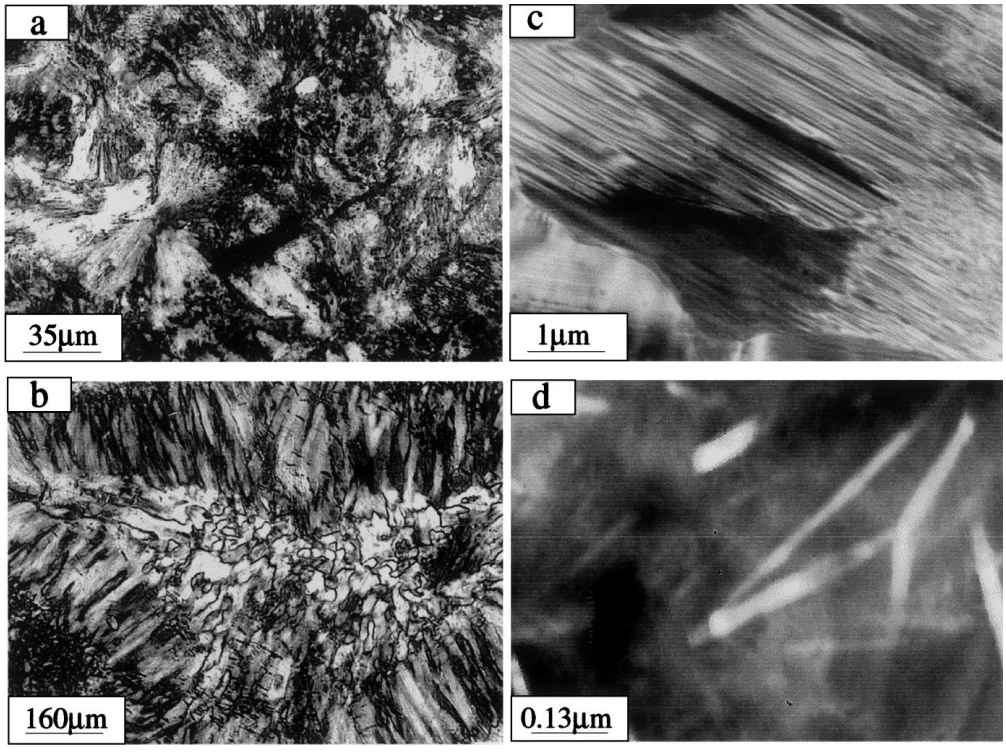

Figure 7 Photomicrographs taken under crossed polarisators of (a) fibrous grain growth, (b) fibre aggregates composed by fibres which project radially outward from small crystals, (c) TEM images of a fine-scale twinned bytownite after hot pressing and deformation, and of (d) those needles which compose the ultra-fine matrix.

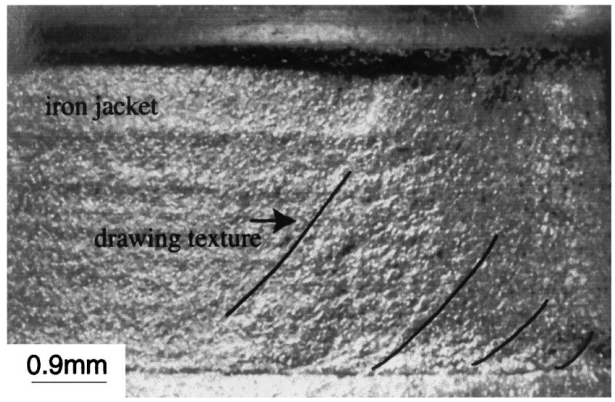

(a)

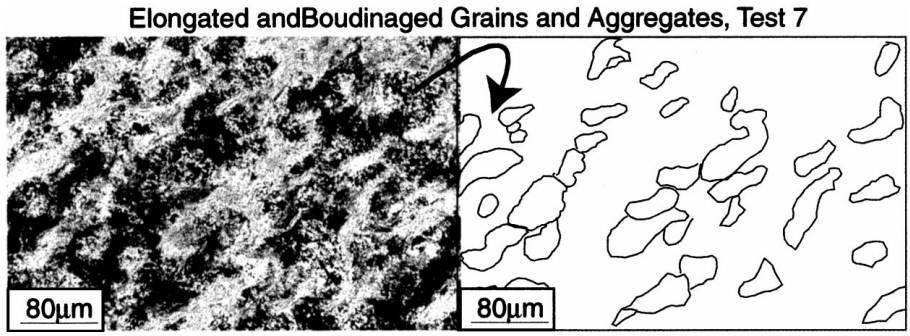

(b)

Figure 8 (a) Drawing texture on the iron jacket after shear deformation (b) Typical microstructures after shear deformation: Grains and aggregates are elongated and boudinaged at 45° to the long axis of the specimen. (Micrograph taken parallel to the long axis of the specimen using crossed polarisators).

around the twisted specimen showed a "drawing texture" after deformation defining a lineation at 45° to the specimen long axis (Fig. 8a). This lineation was also microscopically observed by the shape-orientation of the grains (Fig. 8b). Single grains and grain aggregates were strongly elongated, boudinaged and exhibited sutured grain boundaries (Fig. 8b). Grain sizes increase from about 12 μm in the low strain centre of the specimen to 30 μm in the highly strained outer specimen surface. Strong fibrous grain growth was not observed. TEM imaging still revealed the existence of the ultra-fine matrix composed of nanometer-sized plates.

5.3. Crystallographic Preferred Orientation

In line with the strong deformation features some crystallographic preferred orientation (CPO) development is expected in the deformed bytownite samples. As the grain size is so small, the fabric could not be measured by a conventional U-stage method. However, the presence of a weaker fabric after hot pressing but before deformation and a strong fabric after deformation is indicated from observations of the thins sections using a sensitive first plate under cross polarised light. The *c*-axes of the bytownite crystals are approximately perpendicular to the direction of the principal stress ($\sigma 1$) for the sample deformed by axial compression and approximately at 45° to the long axis of the sample deformed by torsion. The weak CPO in the hot pressed sample might result from the cold pressing or from the hit point tests carried out during hot isostatic pressing. Fabric measurements after cold pressing were not conducted to avoid air contact with the samples. The existence of a strong CPO in the matrix was also confirmed by TEM analyses. TEM generated electron diffraction pattern consisted of a set of well-defined concentric, but hexagonal diffraction rings (Fig. 9) which is typical for oriented superposed diffraction patterns in contrast to diffuse diffraction rings as found for unoriented and amorphous glass phases or for cherts [28].

Figure 9 Electron diffraction pattern of the matrix composed by crystallites after deformation. The set of concentric hexagonal diffraction rings is typical for ultra-fine crystalline material characterised by a preferred crystallographic orientation.

6. Conclusions

The study presented here concerns the fabrication of synthetic samples of defined bytownite composition (An_{80}) suitable for plastic deformation experiments. We showed that

1. Sol-gel derived crystalline or amorphous bytownite is homogeneous in composition, has a low impurity content (<0.5%) and is of very fine grain size after crystallising over a period of 3 days.

2. The hip-ed samples have extremely low water contents.

3. Short (3–5 h) hot isostatic pressing induces very slow grain growth. The density of the sample increases during hot pressing up to 98%.

4. Deformation at high pressure (300 MPa), high temperature (1150 °C, 1200 °C) and constant strain rate (10^{-5} s^{-1}) produces a work-hardening followed by work-softening behaviour for axial compression and a work-hardening behaviour for torsion. The peak stress was attained at strains <10%. The maximum flow stress is a function of the glass content of the sample and the experimental temperature. The strain distributions is inhomogeneous after deformation.

5. Deformation induces microstructures probably due to grain growth under load and semi-plastic flowing.

Acknowledgement

The authors wish to thank St. J. Covey-Crump for reading an earlier manuscript, Ch. Nevado and K. Paech for the precise preparation of thin sections and ion milling, and Ch. Wibberley for correcting the English. Financial support of the Deutsche ForschungsGemeinschaft (DFG/WE1937-1-3) and the Centre National de la Recherche Scientifique (C.N.R.S.) are gratefully acknowledged.

References

1. S. JI, D. MAINPRICE and F. BOUDIER, *J. Struct. Geol.* **10** (1988) 73–81.
2. M. CANNAT, in Proceedings of the Ocean Drilling Program **118** (1991) 399–408.
3. K. E. SEIFERT, *Geol. Soc. Am. Bull.* **80** (1969) 2053–2060.
4. I. Y. BORG and H. C. HEARD, *Contr. Mineral. and Petrol.* **23** (1969) 128–135.
5. I. Y. BORG and H. C. HEARD, in "Experimental and Natural Rock Deformation," edited by P. Paulitsch (1970) pp. 375–403.
6. G. HIRTH and J. TULLIS, *J. Struct. Geol.* **14** (1992) 145–160.
7. J. TULLIS and R. A. YUND, "Fault Mechanics and Transport Properties of Rocks," (1992) pp. 90–117.
8. J. TULLIS and R. A. YUND, *Geology* **13** (1985) 238–241.
9. *Idem., ibid.* **15** (1987) 606–609.
10. *Idem., J. Struct. Geol.* **2** (1980) 439–451.
11. G. L. SHELTON, J. TULLIS and T. E. TULLIS, *Geophys. Res. Letters.* **8** (1981) 55–58.
12. S. M. SCHMID, J. N. BOLAND and M. S. PATERSON, *Tectonophysics* **43** (1977) 257–291.
13. J. TULLIS and R. A. YUND, *J. Struct. Geol.* **13** (1991) 987–1000.
14. S. KARATO and P. WU, *Science* **260** (1993) 771–778.
15. D. L. OLGAARD, in special issue on "Deformation Mechanisms, Rheology and Tectonics" Edited by R. J. Knipe and E. H. Rutter, *Geol. Soc. Spec. Publ.* **54** (1990) 175–181.
16. M. R. DRURY, R. L. M. VISSERS, D. VAN DER WAL and E. H. H. STRATING, *Pure Appl. Geophys.* **137** (1991) 439–460.
17. M. S. PATERSON, "Experimental Rock Deformation," (Springer-Verlag, 1978) p. 254.
18. M. S. PATERSON, *Bull. Mineral* **105** (1982) 20–29.
19. P. N. CHOPRA and M. S. PATERSON, *Tectonophysics* **78** (1981) 453–473.
20. *Idem., J. Geophys. Res.* **89** (1984) 7861–7876.
21. S. KARATO, M. S. PATERSON and J. FITZGERALD, *ibid.* **91** (1986) 8151–8176.
22. R. S. HITCHING, M. S. PATERSON and J. BITMEAD, *Phys. Earth Planet. Inter.* **55** (1989) 277–291.
23. D. L. OLGAARD, M. S. PATERSON, M. CASEY, I. C. STRETTON, M. PIERI and K. KUNZE, *EOS, Transactions AGU* **78** (1997) 46.
24. M. CASEY, K. KUNZE and D. L. OLGAARD, *J. Struc. Geology* **29** (2–3) (1998) 255–267.
25. I. STRETTON and D. L. OLGAARD, *EOS, Transact. AGU*, **78** (1997) 46.
26. M. PIERI and D. L. OLGAARD, *ibid.* **78** (1997) 46.
27. J. HANDIN, D. V. GRIGGS and J. K. O'BRIEN, in special issue on "Rock Deformation" edited by D. V. Griggs, and J. Handin, *Geol. Soc. Am. Mem.* **79** (1960) 245–274.
28. D. MAINPRICE, PhD thesis, Australian National University, Canberra, 1981 pp. 171.

Received 24 December 1998
and accepted 21 April 1999